

# CrystEngComm

Accepted Manuscript



This is an *Accepted Manuscript*, which has been through the Royal Society of Chemistry peer review process and has been accepted for publication.

*Accepted Manuscripts* are published online shortly after acceptance, before technical editing, formatting and proof reading. Using this free service, authors can make their results available to the community, in citable form, before we publish the edited article. We will replace this *Accepted Manuscript* with the edited and formatted *Advance Article* as soon as it is available.

You can find more information about *Accepted Manuscripts* in the [Information for Authors](#).

Please note that technical editing may introduce minor changes to the text and/or graphics, which may alter content. The journal's standard [Terms & Conditions](#) and the [Ethical guidelines](#) still apply. In no event shall the Royal Society of Chemistry be held responsible for any errors or omissions in this *Accepted Manuscript* or any consequences arising from the use of any information it contains.

# Size-Tunable Synthesis and Luminescent Properties of $\text{Gd}(\text{OH})_3:\text{Eu}^{3+}$ and $\text{Gd}_2\text{O}_3:\text{Eu}^{3+}$ Hexagonal Nano-/Microprisms

Guogang Li\*, Yujun Liang, Mengfei Zhang, and Dongyan Yu

*Faculty of Materials Science and Chemistry, China University of Geosciences, Wuhan 430074, P. R. China.*

\*Author to whom any correspondence should be addressed to E-mail: [ggli8312@gmail.com](mailto:ggli8312@gmail.com)

## Abstract

---

Uniform and monodisperse  $\text{Gd}(\text{OH})_3:\text{Eu}^{3+}$  hexagonal prisms were successfully synthesized at a mild condition *via* a large-scale and facile homogeneous coprecipitation process without using any catalysts, surfactants or templates. The size of as-formed  $\text{Gd}(\text{OH})_3:\text{Eu}^{3+}$  precursor prisms could be modulated from micro- to nanoscale by the use of urea and the change of the pH values of the initial solutions. A possible formation mechanism for the  $\text{Gd}(\text{OH})_3:\text{Eu}^{3+}$  hexagonal nano-/microprisms was proposed. After a postannealing process,  $\text{Gd}_2\text{O}_3:\text{Eu}^{3+}$  hexagonal nano-/microprism phosphors with a slight shrinking in size can be transformed from  $\text{Gd}(\text{OH})_3:\text{Eu}^{3+}$ . Both the  $\text{Gd}_2\text{O}_3:\text{Eu}^{3+}$  nanoprisms and microprisms exhibit the same strong red emission corresponding to  ${}^5\text{D}_0 \rightarrow {}^7\text{F}_2$  transition (610 nm) of  $\text{Eu}^{3+}$  under UV light excitation (243 nm) and low-voltage electron beam excitation (1-6 kV). Furthermore, the experimental results indicate that the luminescence properties of the as-obtained phosphors are dependent on their morphologies and sizes. As a result of the controllable morphology and size, and excellent luminescence properties, these  $\text{Gd}_2\text{O}_3:\text{Eu}^{3+}$  nano-/microprism phosphors may find potential applications in optoelectronic devices (fluorescent lamps and field emission displays), bioanalysis and biomedical areas and so on.

---

## 1. Introduction

Recently, there is a growing academic and industrial interest on one-dimensional (1D) nanostructures including rods, wires, tubes and prisms due to their unique optical, electronic and magnetic properties, which mean potential applications in a wide range of fields including nanoscale electronics, photonics, display and advanced bioanalysis.<sup>1</sup> Among various 1D rare earth nanostructures, nanorods/prisms materials are expected to have glamorous characteristics amplified by their well-defined shape, marked shape-specific and quantum size effects.<sup>2</sup> Moreover, the advantageous characteristics of nanorods/prisms are possibly enhanced by modifying surfaces and edges.<sup>3</sup>

On the other hand, rare earth compounds have been widely used in high-performance luminescent devices, catalysts, and other functional materials based on the electronic, optical, and chemical characteristics originating from their 4f electrons.<sup>4</sup> Lanthanum hydroxides, as one of important rare-earth compounds, have been used in lots of fields such as superconductive materials, ceramic, electrode materials, catalyst and sorbent materials, etc.<sup>2, 5</sup> Furthermore, the dehydration of lanthanum hydroxide also provides a straightforward and facile process to obtain lanthanum oxide that is important phosphor host materials.<sup>6</sup> Since a close interrelation between shape, dimension, size and surface of nanomaterials and their chemical and physical properties, mastery over these factors not only enables control of these properties but also enhances their usefulness for a given application.<sup>7</sup> If lanthanum hydroxide were fabricated in the form of 1D nanostructures, they would be expected to be highly functionalized materials as a result of both shape-specific and quantum confinement effects, acting as electrically, magnetically, or optically functional host materials as well. Thus far, many efforts have been made for the preparation of 1D lanthanum hydroxide and oxide nanostructures for advancing their current applications.<sup>8</sup> The widely used method is the catalyst and template-based method. Unfortunately, it generally involves a complicated process and may result in impurities in the products. In order to overcome these difficulties, many recent studies

have demonstrated that wet chemical solution process is one of effective and feasible routes for the synthesis of 1D nanostructures due to low cost, high efficiency and good potential for high-quantity production.<sup>9</sup> For example, there are many reports about 1D lanthanide hydroxides and oxides obtained by a hydrothermal method and postcalcining process. Among them, gadolinium hydroxide has been used as the catalyst and sorbent, and the precursor for the preparation of  $Gd_2O_3$ .<sup>6c, 10</sup> Moreover,  $Eu^{3+}$ -doped  $Gd_2O_3$  phosphor is one of the important red-emitting phosphors. Although the investigations on  $Gd_2O_3:Eu^{3+}$  phosphors are extensive,<sup>9d, 11</sup> few studies have been reported on the synthesis of dispersed, uniform, and well-defined 1D  $Gd_2O_3:Eu^{3+}$  nano-/microprisms and their corresponding luminescent properties. Furthermore, for application at ambient pressure, the hydrothermal reaction is not suitable for large-scale and industrial preparation due to the pressure and cost limitation.<sup>12</sup> So it is significant to develop more facile, efficient, and low-cost techniques to fabricate large-scale and well-crystallized  $Gd(OH)_3:Eu^{3+}$  and  $Gd_2O_3:Eu^{3+}$  hexagonal prisms from microscale to nanoscale.

In this work, we present a simple wet-chemical method for the fabrication of well-defined  $Gd(OH)_3:Eu^{3+}$  hexagonal nano-/microprisms at ambient pressure and low temperature without any catalysts, surfactants or templates. The  $Gd_2O_3:Eu^{3+}$  nano-/microprisms, which inherit their parents' morphology, can be obtained from the calcination of  $Gd(OH)_3:Eu^{3+}$ . The photoluminescent and cathodoluminescent properties of  $Gd_2O_3:Eu^{3+}$  nano-/microprisms for the application as high-performance phosphor as well as the relations with morphology and size were investigated. This novel approach is of significant importance in industrial applications as a consequence of its low costs, benignancy to environment, and synthetic convenience, which makes it promising for the preparation of other oxide-based phosphors.

## 2. Experimental

**Chemicals and materials:** Rare-earth oxides  $Gd_2O_3$  and  $Eu_2O_3$  (all with purity of 99.999%) were purchased from the Science and Technology Parent Company of

Changchun Institute of Applied Chemistry. Urea ( $\text{CO}(\text{NH}_2)_2$ ), nitric acid ( $\text{HNO}_3$ , 65–68 wt-%), ammonia ( $\text{NH}_3 \cdot \text{H}_2\text{O}$ , 25 wt-%) and ethanol were all purchased from the Beijing Fine Chemical Company. All the initial chemicals in this work were of analytical degree reagents and used directly without further purification.

**Preparation:** First,  $\text{Gd}_2\text{O}_3$  and  $\text{Eu}_2\text{O}_3$  were dissolved in dilute  $\text{HNO}_3$ , respectively, forming colorless stock solutions of  $\text{Gd}(\text{NO}_3)_3$  (0.5 M) and  $\text{Eu}(\text{NO}_3)_3$  (0.2 M), respectively. In a typical procedure, stoichiometric  $\text{Gd}(\text{NO}_3)_3$  and  $\text{Eu}(\text{NO}_3)_3$  solution with total  $c(\text{Gd}^{3+} + \text{Eu}^{3+}) = 0.015 \text{ M}$  were added into a 300 mL of aqueous solution. An ammonia solution (25 wt-%) was introduced rapidly into the vigorously stirred solution to adjust its pH from 9 to 11. After vigorous stirring for 10 min, distilled water was added into the solution to make a total volume of 500 mL and the beaker was wrapped with polyethylene film. After additional agitation for 30 min, the mixed solution was heated on a hot plate with strongly stirring to  $80^\circ\text{C}$  within 60 min and then maintained at  $80^\circ\text{C}$  for 2 h. The suspension was cooled to room temperature naturally and the resulting precipitates were separated by centrifugation, and respectively washed with deionized water and anhydrous ethanol in sequence for four times, and then dried at  $80^\circ\text{C}$  in air for 12 h. The as-prepared products at pH = 9 and 11 were denoted as P1 and P2, respectively. The counterparts were prepared by a similar procedure, except for the use of urea ( $\text{CO}(\text{NH}_3)_2$ ), in which the obtained samples were P3 and P4, respectively. Subsequently, the as-synthesized hydroxide precursors were calcined at  $800^\circ\text{C}$  for 2 h in air to obtain the final  $\text{Gd}_2\text{O}_3:\text{Eu}^{3+}$  phosphors, which were correspondingly denoted as P1□-P4□.

**Characterization:** Power X-ray diffraction (XRD) patterns were performed on a D8 Focus diffractometer at a scanning rate of  $10^\circ/\text{min}$  in the  $2\theta$  range from  $10^\circ$  to  $80^\circ$ , with graphite-monochromatized Cu  $K\alpha$  radiation ( $\lambda = 0.15405 \text{ nm}$ ). TGA-DSC (thermogravimetric analysis and differential scanning calorimetry) curves were recorded with a thermal analysis instrument (SDT 2960, TA Instruments, New Castle, DE) with a heating rate of  $10^\circ\text{C}/\text{min}$  in an air flow of 100 mL/min. The morphology and composition of the samples were inspected using a field emission scanning electron microscopy (FE-SEM, S-4800, Hitachi). Nitrogen adsorption/desorption

analysis was measured using a Micromeritics ASAP 2020 M apparatus. The specific surface area was determined by the Brunauer–Emmett–Teller (BET) method. Low- to high-resolution transmission electron microscopy (TEM) and selected area electron diffraction (SAED) patterns were recorded using a FEI Tecnai G2 S-Twin with a field emission gun operating at 200 kV. Images were acquired digitally on a Gatan multiplane CCD camera. Photoluminescence (PL) excitation and emission spectra were recorded with a Hitachi F-4500 spectrophotometer equipped with a 150W xenon lamp as the excitation source. Cathodoluminescence (CL) measurements were carried out in an ultra-highvacuum chamber ( $< 10^{-8}$  Torr), where the phosphors were excited by an electron beam in the voltage range of 0.5–6.0 kV and different filament currents, and the emission spectra were recorded using an F-4500 spectrophotometer. The PL lifetimes of the samples were measured with a Lecroy Wave Runner 6100 Digital Oscilloscope (1GHz) using a tunable laser (pulse width 4 ns) as the excitation source (Continuum Sunlite OPO). All the measurements were performed at room temperature (RT).

### 3. Results and Discussion

#### 3.1 Phase Purity, Morphology, and Formation Mechanism of $\text{Gd}(\text{OH})_3:\text{Eu}^{3+}$ Nano-/Microprisms

The composition and phase purity of the as-prepared  $\text{Gd}(\text{OH})_3:\text{Eu}^{3+}$  products were first examined by XRD. Figure 1 shows the XRD patterns of the  $\text{Gd}(\text{OH})_3:\text{Eu}^{3+}$  products (P1-P4) prepared by homogenous precipitation process at 80°C for 2 h with different pH values and dosage of  $\text{CO}(\text{NH}_2)_2$  conditions. The X-ray diffraction peaks of P1-P4 are readily indexed to the pure hexagonal phase of  $\text{Gd}(\text{OH})_3$  [space group:  $P63/m(176)$ ], which coincides well with the literature values (JCPDS No.38-1042). Except for some minor diffraction peaks at about 37.6° and 53.2° that should be attributed to  $\text{Eu}(\text{OH})_3$ , no obvious peaks shift and impurity phases appear at current doping level, indicating the high purity of the as-prepared  $\text{Gd}(\text{OH})_3:\text{Eu}^{3+}$  products and the homogenous doping of  $\text{Eu}^{3+}$  ions into  $\text{Gd}(\text{OH})_3$  host by substituting of  $\text{Gd}^{3+}$  ions.

As we know, the difference in the relative intensity of crystal diffraction peaks reflects the difference in growth orientation of crystal.<sup>13</sup> The XRD patterns of P1-P4 products in Figure 1 show a little differences in the relative intensities based on (100), (110) and (101) diffraction peaks, indicative of the different growth orientation or rate under different pH and urea conditions. This also indirectly confirms that  $\text{Gd}(\text{OH})_3:\text{Eu}^{3+}$  prisms with different surfaces and sizes can be obtained through changing external experimental conditions.

SEM images can provide direct information on the shapes and sizes of the as-prepared  $\text{Gd}(\text{OH})_3:\text{Eu}^{3+}$  products grown under different experimental conditions. The morphologies and dimensions of the representative  $\text{Gd}(\text{OH})_3:\text{Eu}^{3+}$  products (P1-P4) are summarized in Table 1. From Table 1, it is clearly seen that the pH values of the initial reaction system and the use of  $\text{CO}(\text{NH}_2)_2$  have great influence on the shapes and sizes of  $\text{Gd}(\text{OH})_3:\text{Eu}^{3+}$  crystals, which will be discussed in the following paragraphs.

Figure 2 shows the typical SEM images of  $\text{Gd}(\text{OH})_3:\text{Eu}^{3+}$  products prepared at the absence of urea with different pH values. The product obtained at pH = 9 (P1) is composed of monodisperse hexagonal submicprisms with height of prism ( $L$ ) and hexagonal side length ( $D$ ) about 0.40  $\mu\text{m}$  and 0.09–0.15  $\mu\text{m}$ , respectively. When the pH of the initial solution is adjusted to pH = 11, the product P2 remained the morphology of hexagonal prisms. However, its size greatly increase to  $L = \sim 1.45 \mu\text{m}$  and  $D = 0.20\text{--}0.25 \mu\text{m}$ , respectively, as shown in Figure 2c and Table 1. Moreover, the increased rate of  $L$  is higher than that of  $D$ . A careful observation on single  $\text{Gd}(\text{OH})_3:\text{Eu}^{3+}$  submicroprism and microprism reveals that they consists of the smaller nanoparticles (Figure 2b and 2d). Furthermore, the cross-sectional view of P1 and P2 products exhibit the formation of perfect hexagonal prisms, as shown by the yellow hexagons and in Figure 2b and 2d. TEM images also show that the as-formed  $\text{Eu}^{3+}$  ion doped gadolinium hydroxide products represent prism-like morphology (Figure 2e), which is consistent with SEM observation. The crystal structure of the individual microprism of P2 is further characterized by HRTEM. The HRTEM image of a part of single microprism (Figure 2f) shows a perfect crystallinity of the lattice planes. The



lattice fringes show the imaging characteristics of hexagonal  $\text{Gd}(\text{OH})_3$  crystal, in which the  $d$  spacing of 1.55 nm corresponds to the distance between the (220) planes, and thus the preferential growth direction is [001].<sup>9d, 12</sup> The corresponding Fourier transform electron diffraction pattern of P2 (Figure 2f, inset) also reveals a single-crystalline structure of this product and the diffraction spots can be indexed to a pure hexagonal phase of  $\text{Gd}(\text{OH})_3$  with space group  $P63/m(176)$ . The chemical composition of the as-prepared products was analyzed by EDX spectroscopy. According to the EDX spectrum of the representative P2 product taken in the SEM mode (Figure 2g), no elements other than Gd, O, Eu are present from measurement (H element cannot be detected by EDX measurement). Furthermore, the EDX spectrum show an approximate atomic ratio of 1 : 3 for (Gd, Eu) : O, which match well with that of gadolinium hydroxide within the experimental error of EDX experiments. The EDX analysis gives further support for the XRD results.

After adding  $\text{CO}(\text{NH}_2)_2$  into the reaction system, the as-prepared products at different pH values also present prism-like shapes, as shown in Figure 3. At pH = 9, the product P3 consists of a great deal of irregular hexagonal nanoprisms (Figure 3a), suggesting the high yield and good uniformity achieved with this approach. The average  $L$  and  $D$  of these nanoprisms are about 0.20 and 0.06  $\mu\text{m}$ , respectively. Interestingly, the top/bottom surfaces exhibit concave centers (Figure 3b). When the pH value is adjusted to 11 with  $\text{NH}_3\cdot\text{H}_2\text{O}$  (25 wt.-%), the morphology of the product P4 is still nanoprisms with remarkable uniformity and monodispersity (Figure 3c). Furthermore, the center of the prisms is still concave (Figure 3d and inset), similar to P3. Although the morphology of is same, the size of the P4 product varies greatly compared with that of P3 product, which has an average size of 0.30  $\mu\text{m}$  in  $L$  and 0.65  $\mu\text{m}$  in  $D$ , respectively. Obviously, there is also an increase in the size of products with enhancing the pH values from 9 to 11 at the presence of  $\text{CO}(\text{NH}_2)_2$ , which is same to the previous result of P1 and P2. The inset in Figure 3d is a high-magnification SEM image of single hexagonal nanoprism perpendicular to the substrate. The very regular hexagonal cross section can be clearly observed. Meanwhile, the representative TEM image of P3 is shown in Figure 3e. It is found that the contrast between the edge parts

and the central part further confirms the uniformity and monodispersity of P3 product. As disclosed by the corresponding HRTEM image (Figure 3f) that was taken with the electron beam perpendicular to the edge of the nanoprisms, the product is structurally uniform with interplanar distances of about 1.56 nm, which corresponds to the d-spacing value of the (220) planes. Therefore, it is concluded that the preferential growth direction is [001]. The diffraction spots (Figure 3f, inset) obtained from Fourier transform electron diffraction pattern of P3 can be indexed to a pure hexagonal phase of  $\text{Gd}(\text{OH})_3$ . In summary, the  $\text{Gd}(\text{OH})_3:\text{Eu}^{3+}$  products undergo the variations from microprisms to nanoprisms compared with P1 and P2, and P3 and P4, respectively. Because all the experimental parameters were identical from P1 to P2 and from P3 to P4 products except for the pH values of the initial reaction solution, the different sizes of the  $\text{Gd}(\text{OH})_3:\text{Eu}^{3+}$  products should be attributed to the variation of the pH values. This can be explained by the complex interaction and balance between the chemical potential and the rate of ionic motion. A higher pH value implies a higher  $\text{OH}^-$  ion concentration and a higher chemical potential in solution. A high chemical potential is preferable for the growth of higher aspect ratio 1D structure (Table 1). The phenomenon is similar to the connection of pH values with the aspect ratio of 1D structures in the work of Wang and Li et al.<sup>2</sup> Furthermore, each nanoprism or microprism has a uniform hexagonal side length along its entire length and the c-axis (corresponding to the growth direction of the prisms) ends project out, indicating the growth anisotropy in the c-axis is strictly maintained throughout the process. In particular, no branching is observed, which implies that the  $\text{Gd}(\text{OH})_3:\text{Eu}^{3+}$  nanoprisms or microprisms were grown from spontaneous nucleation with high crystal perfection.<sup>9d, 14</sup> Generally, various well-defined, uniform and monodisperse hexagonal prisms of  $\text{Gd}(\text{OH})_3:\text{Eu}^{3+}$  products could be synthesized by simply adjusting the pH of the initial reaction system.

Except for the pH effect, the use of  $\text{CO}(\text{NH}_2)_2$  has great effects on the size and morphology of the homogenous precipitation products. Comparing P1 with P3, or P2 with P4, it is easily observed that some of crystal defects appear on the surface of  $\text{Gd}(\text{OH})_3:\text{Eu}^{3+}$  nanoprisms (Figure 3b and 3d). This implies that the growth of

nanoprisms occurred from several nucleation centers possibly results in anisotropic defective structure, which is similar to the case of mesocrystals formation.<sup>15</sup> At the same time, the use of  $\text{CO}(\text{NH}_2)_2$  obviously reduce the size of prisms from microscale to nanoscale, as shown in Table 1. The possible reason is that  $\text{NH}_4^+$  ions can be selectively adsorbed on specific facets of the initial  $\text{Gd}(\text{OH})_3:\text{Eu}^{3+}$  crystal seeds and change their surface energy, and thus have a guiding effect on changes in the prisms of the as-prepared  $\text{Gd}(\text{OH})_3:\text{Eu}^{3+}$  crystals. The higher  $\text{NH}_4^+$  ion concentrations (from the hydrolysis of  $\text{CO}(\text{NH}_2)_2$ ) may greatly reduce the ionic motion rate of  $\text{Gd}^{3+}$  ion, giving a low aspect ratio. Some researchers had suggested that the simple ions such as  $\text{K}^+$ ,  $\text{H}^+$ ,  $\text{NH}_4^+$ ,  $\text{Na}^+$ ,  $\text{Rb}^+$ ,  $\text{Cs}^+$  and so on direct the growth of nanoparticles into different shapes, highlighting the importance of these species.<sup>16</sup> It is therefore reasonable to assume a similar situation for the effects of  $\text{NH}_4^+$  on the morphologies and sizes. In addition, besides providing basic media for precipitation,  $\text{NH}_3\cdot\text{H}_2\text{O}$  and  $\text{CO}(\text{NH}_2)_2$  could also coordinate with  $\text{Gd}^{3+}$  ions to form  $\text{Gd}(\text{NH}_3)_x^{3+}$  and  $\text{Gd}(\text{CO}(\text{NH}_2)_2)_x^{3+}$  complexes, which influences the transportation of  $\text{Gd}^{3+}$  ions to the growing sites of the crystal seeds. Therefore, the morphologies and sizes of the products obtained at the absence and presence of  $\text{CO}(\text{NH}_2)_2$  are distinctly different. In summary, the final crystal shapes, sizes and the aspect ratios of the as-synthesized products are strongly related to the pH conditions and the dosage of urea.

In general, the growth of  $\text{Gd}(\text{OH})_3:\text{Eu}^{3+}$  crystals with various morphologies and sizes is a complex process, which is the cooperative result of inherent structures and external experimental conditions such as pH values of the initial solution, dosage of  $\text{CO}(\text{NH}_2)_2$ . Based on the above experimental results, the formation and evolution mechanisms of  $\text{Gd}(\text{OH})_3$  nano-/microprisms are proposed as follow: Firstly, the mix of  $\text{Gd}(\text{NO}_3)_3$  with  $\text{NH}_3\cdot\text{H}_2\text{O}$  or  $\text{CO}(\text{NH}_2)_2$  achieve a metastable supersaturated solution; Then large numbers of  $\text{Gd}(\text{OH})_3$  crystal nucleations (namely colloid particles) forms through a continuously stir and heat process; Next, these colloid particles subsequently dissolve and recrystallize to form hexagonal seeds of  $\text{Gd}(\text{OH})_3$ ; Finally, they grow into uniform, crystalline prism-like structure along the c-axis due to a highly anisotropic hexagonal structure. A possible formation process of  $\text{Gd}(\text{OH})_3$

nano-/microprisms is simply shown in Scheme 1. As we know, the lanthanide hydroxides mostly have hexagonal crystal structures, which is well-known for its anisotropic growth nature. A rapid adjustment of the pH value of the solution by  $\text{NH}_3 \cdot \text{H}_2\text{O}$  and the use of  $\text{CO}(\text{NH}_2)_2$  leads to the formation of a white precipitate which immediately appears in solution. This feeding mode can be regarded as a similar process to the “injection” technique adopted by Peng et al.,<sup>17</sup> which will ensure a higher monomer concentration so that the obtained precipitates will have many anisotropic seeds for the following homogenous precipitation process. During the homogenous precipitation process,  $\text{Gd}(\text{OH})_3$  colloidal particles act as the intermediates to form hexagonal crystal seeds that can further induce anisotropic growth along crystallographically reactive directions (c-axis), which is critical in the synthesis of the  $\text{Gd}(\text{OH})_3$  prism-like structure.<sup>2, 9d</sup> In addition, although hexagonal  $\text{Gd}(\text{OH})_3$  crystal seeds have a preferential orientation growth along [001] direction, its growth rate varies with the absence and presence of  $\text{CO}(\text{NH}_2)_2$ . This might lead the size of these prisms can be adjusted from microscale to nanoscale. It is worth pointing out that the doping of  $\text{Eu}^{3+}$  into the  $\text{Gd}(\text{OH})_3$  host did not change the phase, crystallization, and morphology due to a low doping amount and the same hexagonal phase structure. Thus,  $\text{Gd}(\text{OH})_3 \cdot \text{Eu}^{3+}$  nano-/microprisms can be prepared through the same homogenous precipitation process.

### 3.2. Crystallization Behavior, Morphologies and Luminescence Properties of $\text{Gd}_2\text{O}_3 \cdot \text{Eu}^{3+}$ Nano-/Microprisms

Thermal decomposition of the homogeneously precipitated/hydrothermal precursors is a facile and usual route toward tailored rare earth and metal oxides.<sup>18</sup> After the synthesis of prism-like  $\text{Gd}(\text{OH})_3 \cdot \text{Eu}^{3+}$  precursors, P2 was employed to investigate the effect of calcinations on the crystallization and morphology of the as-prepared products. Figure 4 shows the TGA-DSC curves of  $\text{Gd}(\text{OH})_3 \cdot \text{Eu}^{3+}$  crystals (P2) prepared at 80°C. Obviously, there are two major stages of rapid weight loss in the TGA curve at about 325°C and 427°C, accompanying their corresponding endothermic peaks. It demonstrates that the transformation from  $\text{Gd}(\text{OH})_3 \cdot \text{Eu}^{3+}$  to  $\text{Gd}_2\text{O}_3 \cdot \text{Eu}^{3+}$  undergo two steps, and there may exist an intermediate phase other than

Gd(OH)<sub>3</sub> and Gd<sub>2</sub>O<sub>3</sub>. The weight losses for the two stages are 9.42% and 3.45%, respectively. The total weight loss (12.87%) is in basic agreement with the theoretical value of Gd(OH)<sub>3</sub> (12.98%), calculated from the reaction of its complete dehydration to produce Gd<sub>2</sub>O<sub>3</sub>. Since most of the rare earth compounds can exist in the form of LnOOH, the dehydration process can be supposed to be two steps: Gd(OH)<sub>3</sub> → GdOOH + H<sub>2</sub>O and 2GdOOH → Gd<sub>2</sub>O<sub>3</sub> + H<sub>2</sub>O. The theoretical weight loss for the two processes is 8.65% and 4.73%, respectively, which is quite close to the data that we have obtained from the TGA curve. The results mentioned above are consistent with the previous literature.<sup>9d, 19</sup> According to the TG-DSC results, the as-prepared P2 product was calcined at 800 °C for 2 h to obtain gadolinium oxide, and the obtained white powders were denoted as P2□. All diffraction peaks of P2□ in Figure 5a can be assigned to pure Gd<sub>2</sub>O<sub>3</sub> cubic phase [Space group: *Ia-3* (206)], which coincides very well with JCPDS No.05-0602. No second phase appears, indicating that the Gd(OH)<sub>3</sub>:5 mol% Eu<sup>3+</sup> (P2) was completely converted to Gd<sub>2</sub>O<sub>3</sub>:5 mol% Eu<sup>3+</sup> (P2□) at 800 °C. Figure 5b-4e shows typical SEM, TEM, HRTEM and SAED images of Gd<sub>2</sub>O<sub>3</sub>:5 mol% Eu<sup>3+</sup> product, respectively. From Figure 5b and 4c, it can be seen that the Gd<sub>2</sub>O<sub>3</sub>:5 mol% Eu<sup>3+</sup> inherited their parents' morphologies. The morphologies were maintained perhaps due to the higher activation energies needed for the collapse of these structures.<sup>18</sup> However, their surface became rough and appeared a slight shrink in size in comparison with Gd(OH)<sub>3</sub>:5 mol% Eu<sup>3+</sup>. This might result from the gradual elimination of H<sub>2</sub>O and CO<sub>2</sub> during the calcinations process. In general, the conversion did not lead to the change in the morphologies. Such a transformation was common for rare earth hydroxide and other metal compounds decomposing.<sup>18</sup> The fine structures of P2□ were studied by HRTEM and SAED techniques. Figure 5d shows its HRTEM image, in which the lattice fringes show the imaging characteristics of the Gd<sub>2</sub>O<sub>3</sub> cubic phase where the d spacing of 3.13 Å corresponds to the distance of the (222) plane. The corresponding SAED pattern (Figure 5e) taken from a single prism can be indexed as the (211), (222), (322), and (411) reflections of the cubic Gd<sub>2</sub>O<sub>3</sub>. These results further confirm the presence of highly crystalline Gd<sub>2</sub>O<sub>3</sub> phase after annealing the Gd(OH)<sub>3</sub>:Eu<sup>3+</sup> at suitable temperature, agreeing well

with the XRD results.

The trivalent europium ion ( $\text{Eu}^{3+}$ ) is well-known as a red-emitting activator due to its  $^5\text{D}_0$ - $^7\text{F}_J$  transitions ( $J = 0, 1, 2, 3, 4$ , usually ranging from 578 nm for  $J = 0$  to 700 nm for  $J = 4$ , with  $^5\text{D}_0$ - $^7\text{F}_2$  around 610–625 nm as the most prominent group).<sup>11</sup> These emission lines have found an important application in the lighting (such as  $\text{Y}_2\text{O}_3:\text{Eu}^{3+}$  and  $\text{YVO}_4:\text{Eu}^{3+}$  used in lamps) and display (such as  $\text{Y}_2\text{O}_2\text{S}:\text{Eu}^{3+}$  used in color television) fields. It is well known that  $\text{Eu}^{3+}$ -activated  $\text{Gd}_2\text{O}_3$  phosphor is one of the important commercial red-emitting phosphors under the excitation of ultraviolet light (UV) and electron beam. The measurements of photoluminescent (PL) properties are performed on the as-synthesized  $\text{Gd}_2\text{O}_3:5 \text{ mol}\% \text{Eu}^{3+}$  at room temperature. Figure 6a and 6b show the PL excitation and emission spectra of P2□ product, respectively. The excitation spectrum monitored wavelength at 613 nm shows a broad band from 200 to 300 nm with a maximum at 243 nm and some weak transitions between 300 and 500 nm. The strong broad band centered at 243 nm is due to the charge transfer band (CTB) of  $\text{Eu}^{3+}-\text{O}^{2-}$ , and the weak lines between 300 and 500 nm can be ascribed to the characteristic  $f-f$  transitions of  $\text{Eu}^{3+}$  within its  $4f^6$  configuration. Other weak peaks at 275 nm and 309 nm should be indexed to the characteristic transitions  $^8\text{S}-^6\text{I}$  and  $^8\text{S}-^6\text{P}$  of  $\text{Gd}^{3+}$  ions, respectively. Upon excitation with 280 nm UV, the  $\text{Gd}_2\text{O}_3:5 \text{ mol}\% \text{Eu}^{3+}$  (P2□) product shows a strong red luminescence with the CIE (Commission Internationale de l'Eclairage 1931 chromaticity) chromaticity coordinates (0.575, 0.350), and the corresponding emission spectrum consists of the characteristic transitions of  $\text{Eu}^{3+}$  within its  $4f^6$  configuration, i.e.,  $^5\text{D}_1 \rightarrow ^7\text{F}_1$  (535 nm),  $^5\text{D}_0 \rightarrow ^7\text{F}_0$  (582 nm),  $^5\text{D}_0 \rightarrow ^7\text{F}_1$  (589, 594 nm),  $^5\text{D}_0 \rightarrow ^7\text{F}_2$  (613, 629 nm),  $^5\text{D}_0 \rightarrow ^7\text{F}_3$  (653 nm). The strongest one is located at 613 nm. The decay curve for the luminescence of  $\text{Eu}^{3+}$  (monitored by  $^5\text{D}_0 \rightarrow ^7\text{F}_2$ , 613 nm) can be well fitted into single-exponential function (Figure 7), and the lifetimes for the  $^5\text{D}_0$  lowest excited state of  $\text{Eu}^{3+}$  are determined to be 2.19, 1.54, 2.52 and 2.59 ms for P1□- P4□, respectively, basically agreeing with the reported values for other  $\text{Eu}^{3+}$ -doped  $\text{Gd}_2\text{O}_3$  systems.<sup>20</sup>

In order to investigate the effect of morphology and size of  $\text{Gd}_2\text{O}_3:5 \text{ mol}\% \text{Eu}^{3+}$  nano-/microprisms on its luminescent properties. The comparison of PL emission

intensity of as-synthesized  $\text{Eu}^{3+}$ -doped  $\text{Gd}_2\text{O}_3$  prism-like phosphors with different sizes (excited at 243 nm) is shown in Figure 6c. It should be mentioned that all the experimental conditions were kept identical in order to avoid experimental errors. From Figure 6c, it can be seen that the microprism phosphor (P2□) has a higher PL intensity than that of submicroprism and nanoprism phosphors (P1□-P3□). It is well-known that the surface area of the materials increases with a decrease in the size. The large surface area results in a large number of defects into the phosphor crystal, which have serious impairment in the PL intensity for phosphors because they provide nonradiative recombination routes for electrons and holes. In order to be as efficient as possible for the phosphors, the number of electron/hole recombinations via optically active centers must be maximized. If the surface area is greatly reduced by increasing crystallite size, the phosphor with fewer defects would show great improvement in the PL intensity.<sup>21</sup> Herein, the surface area of the as-synthesized  $\text{Gd}_2\text{O}_3:\text{Eu}^{3+}$  microprisms is much smaller than that of  $\text{Gd}_2\text{O}_3:\text{Eu}^{3+}$  nanoprisms because the former is much bigger than the latter in size (Table 1). Therefore, a large number of electrons and holes in the excited state will return to ground state via optically radiative recombination routes for microprism phosphors. This is the reason that the PL intensity of the microprism phosphor (P2□) has a higher PL intensity than that of submicroprism and nanoprism phosphors (P1□-P3□). The specific surface area determined by the Brunauer-Emmett-Teller method on the representative P2□ and P4□ products were 21.05 and 15.22  $\text{m}^2/\text{g}$  (Figure 8), respectively, which further supports the above conclusion.

The field emission displays (FEDs) have gained a great interest and have been recognized as one of the most promising technologies in the flat panel displays (FPDs) market due to their most important features like great brightness, wide horizontal and vertical view angles, good contrast ratio, high efficiency with a low power consumption, short response time, and wide work temperature range.<sup>22</sup> In the development of FEDs, phosphors are irreplaceable components for preparing field emission display devices. The successful employment of the FED technique in the practical application requires the development of phosphors which show high current

density, high efficiency and good stability at low electron voltage excitation. Moreover, resolution is a pivotal index for display, which is closely related to the particle size of the phosphors and thus smaller particles are propitious to higher resolution.<sup>23</sup> To explore the potential application of the prism-like  $\text{Gd}_2\text{O}_3:\text{Eu}^{3+}$  phosphors as cathodoluminescent material, we investigate their CL properties in detail. The CL spectra profiles for the representative P2□ and P4□ phosphors basically agree with those of PL emission spectra, as shown in Figure 9. Under low-voltage electron-beam excitation ( $V_a = 4.0$  kV,  $J_a = 80$   $\mu\text{A}/\text{m}^2$ ), the representative P2□ and P4□ phosphor shows a strong red luminescence to the naked eye, and the obtained CL spectra consists of the characteristic transitions of  $\text{Eu}^{3+}$  ion within its  $4f^6$  configuration. The strongest one is located at 613 nm corresponding to the  ${}^5\text{D}_0 \rightarrow {}^7\text{F}_2$  transition of  $\text{Eu}^{3+}$ . Moreover, the CL intensity of P2□ was higher than that of P4□ under the same excitation condition, which was also due to different surface area and defects. This is consistent with their PL comparative result. In addition, the CL emission intensities of the of P2□ microprism phosphor has been representatively investigated as a function of the anode current density ( $J_a$ ) and anode voltage ( $V_a$ ), as shown in Figure 9. When the anode voltage is fixed at 5.0 kV, the CL intensity increases with raising the  $J_a$  from 20 to 120  $\mu\text{A}/\text{m}^2$  (Figure 9a). Similarly, under the  $J_a = 80$   $\mu\text{A}/\text{m}^2$  electron-beam excitation, the CL intensity also increases with increasing the  $V_a$  from 1.0 to 6.0 kV (Figure 9b). There is no obvious saturation trend in the CL intensity of P2□ phosphor with the increase of  $V_a$  and  $J_a$ , indicating promising properties for application in field emission display devices. The increase in CL brightness with an increase in electron energy and filament current is attributed to the deeper penetration of the electrons into the phosphor body and the larger electron-beam current density. The electron penetration depth can be estimated using the empirical formula:

$$L[\text{\AA}] = 250 \left( \frac{A}{\rho} \right) \left( \frac{E}{\sqrt{Z}} \right)^n, n = \frac{1.2}{1 - 0.29 \lg Z}$$

where  $n = 1.2/(1 - 0.29 \lg Z)$ , and  $A$  is the atomic or molecular weight of the material,  $\rho$  is the bulk density,  $Z$  is the atomic number or the number of electrons per molecule in the compounds, and  $E$  is the accelerating voltage (kV).<sup>24</sup> For  $\text{Gd}_2\text{O}_3:5$  mol%  $\text{Eu}^{3+}$



microprism phosphors,  $Z = 152$ ,  $A = 361.97$  g/mol,  $\rho = 7.62$  g/cm<sup>3</sup>, the estimated electron penetration depth at 3.0 kV is about 6.3 nm. For CL, the Eu<sup>3+</sup> ions are excited by the plasma produced by the incident electrons. The deeper the electron penetration depth, the more plasma will be produced, which results in more Eu<sup>3+</sup> ions being excited and thus the CL intensity increases.

#### 4. Conclusion

In summary, the fine, uniform, and monodisperse Gd(OH)<sub>3</sub>:Eu<sup>3+</sup> nano-/microprisms have been successfully prepared through a large-scale, facile and general homogenous precipitation method. It is found that the change of pH can increase the size of prisms, whereas the use of CO(NH<sub>2</sub>)<sub>2</sub> obviously reduce their sizes. Therefore, the size of the prism-like Gd(OH)<sub>3</sub>:Eu<sup>3+</sup> precursors could be modulated from micro- to nanoscale. The possible formation mechanisms have been proposed on an anisotropic growth nature resulting from the hexagonal crystal structure of lanthanide hydroxides. Through a heat treatment, the corresponding Gd<sub>2</sub>O<sub>3</sub>:Eu<sup>3+</sup> nano-/microprisms, which maintain their parents' morphology, can be obtained by thermal transformation from the Gd(OH)<sub>3</sub>:Eu<sup>3+</sup>. The PL, CL as well as the kinetic decay properties of Gd<sub>2</sub>O<sub>3</sub>:Eu<sup>3+</sup> nano-/microprisms phosphors are investigated in detail. The experimental results indicate that the luminescent properties of Gd<sub>2</sub>O<sub>3</sub>:Eu<sup>3+</sup> nano-/microprisms phosphors are strongly dependent on their morphologies and sizes, which result from different surface areas and defects. Due to the strong red emission corresponding to the <sup>5</sup>D<sub>0</sub>→<sup>7</sup>F<sub>2</sub> transition (613 nm) of Eu<sup>3+</sup> under UV excitation (243 nm) and low-voltage electron beams excitation (1-6 kV) and excellent dispersing properties of the obtained Gd<sub>2</sub>O<sub>3</sub>:Eu<sup>3+</sup> nano-/microprisms phosphors, they are potentially applied in fluorescent lamps and field emission display devices. Moreover, this general, simple, green, and high-yield method may be of much significance in the synthesis of many other one-dimensional hydroxides and oxides.

## Acknowledgments

This project is financially supported by the National Natural Science Foundation of China (Grant Nos. NSFC 21301162, 21171152) and the Fundamental Research Funds for the Central Universities, China University of Geosciences (Wuhan) (Grant Nos. CUG 130402).

## Notes and References:

- 1 (a) Y. N. Xia, P. D. Yang, Y. G. Sun, Y. Y. Wu, B. Mayers, B. Gates, Y. D. Yin, F. Kim and H. Q. Yan, *Adv. Mater.*, 2003, **15**, 353; (b) R. C. Jin, Y. W. Cao, C. A. Mirkin, K. L. Kelly, G. C. Schatz and J. Zheng, *Science*, 2001, **294**, 1901; (c) Z. Y. Hou, G. G. Li, H. Z. Lian and J. Lin, *J. Mater. Chem.*, 2012, **22**, 5254; (d) L. Xu, H. W. Song, B. Dong, Y. Wang, X. Bai, G. L. Wang and Q. Liu, *J. Phys. Chem. C*, 2009, **113**, 9609; (e) M. Bockrath, W. Liang, D. Bozovic, J. H. Hafner, C. M. Lieber, M. Tinkham and H. Park, *Science*, 2001, **291**, 283; (f) Y. Huang, X. F. Quan, Q. Q. Wei and C. M. Lieber, *Science*, 2001, **291**, 851; (g) S. Y. Song, Y. Zhang, Y. Xing, C. Wang, J. Feng, W. D. Shi, G. L. Zheng and H. J. Zhang, *Adv. Funct. Mater.*, 2008, **18**, 2328; (h) S. Y. Song, Y. Zhang, J. Feng, X. Ge, D. P. Liu, W. Q. Fan, Y. Q. Lei, Y. Xing and H. J. Zhang, *CrystEngComm.*, 2009, **11**, 1987.
- 2 (a) X. Wang and Y. D. Li, *Angew. Chem., Int. Ed.*, 2002, **41**, 4790; (b) S. Y. Song, J. P. Fu, X. Y. Li, W. Gao and H. J. Zhang, *Chem.-Eur. J.*, 2013, **19**, 2889.
- 3 (a) H. W. Song, L. X. Yu and S. Z. Lu, *Opt. Lett.*, 2005, **30**, 483; (b) H. Zhang, H. W. Song and H. Q. Yu, *J. Phys. Chem. C*, 2007, **111**, 6524; (c) S. L. Gai, C. X. Li, P. P. Yang and J. Lin, *Chem. Rev.*, 2014, **114**, 2343.
- 4 (a) Z. G. Yan and C. H. Yan, *J. Mater. Chem.*, 2008, **18**, 5046; (b) J. Lin, M. Yu, C. K. Lin and X. M. Liu, *J. Phys. Chem. C*, 2007, **111**, 5835; (c) M. S. Palmer, M. Neurock and M. M. Olken, *J. Am. Chem. Soc.*, 2002, **124**, 8452; (d) Y. Hasegawa, S. Thongchant, Y. Wada, H. Tanaka, T. Kawai, T. Sakata, H. Mori and S. Yanagida, *Angew. Chem.*, 2002, **114**, 2177; (e) K. S. Sohn, Y. G. Choi, Y. Y. Choi and H. D.

- Park, *J. Electrochem. Soc.*, 2000, **147**, 3552; (f) K. S. Sohn, Y. Y. Choi, H. D. Park and Y. G. Choi, *J. Electrochem. Soc.*, 2000, **147**, 2375; (g) C. C. Lin and R. S. Liu, *J. Phys. Chem. Lett.*, 2011, **2**, 1268; (h) D. T. Tu, W. Zheng, Y. S. Liu, H. M. Zhu, X. Y. Chen, *Coord. Chem. Rev.*, (2013), <http://dx.doi.org/10.1016/j.ccr.2013.11.017>.
- 5 (a) Q. Tang, Z. P. Liu, S. Li, S. Y. Zhang, X. M. Liu and Y. T. Qian, *J. Cryst. Growth*, 2003, **259**, 208; (b) A. W. Xu, Y. P. Fang, L. P. You and H. Q. Liu, *J. Am. Chem. Soc.*, 2003, **125**, 1494; (c) X. Wang and Y. D. Li, *Chem.-Eur. J.*, 2003, **9**, 5627; (d) J. C. Wang, Q. Liu and Q. F. Liu, *J. Mater. Chem.*, 2005, **15**, 4141; (e) Y. P. Fang, A. W. Xu, L. P. You, R. Q. Song, J. C. Yu, H. X. Zhang, Q. Li and Z. Q. Liu, *Adv. Funct. Mater.*, 2003, **13**, 955; (f) J. Zhang, Z. G. Liu, J. Lin and J. Fang, *Cryst. Growth Des.*, 2005, **5**, 1527; (g) A. Tsubouchi and T. C. Bruice, *J. Am. Chem. Soc.*, 1995, **117**, 7399; (h) P. P. Yang, S. Gai and J. Lin, *Chem. Soc. Rev.*, 2012, **41**, 3679.
- 6 (a) H. Q. Liu, L. L. Wang, S. Q. Chen and B. S. Zou, *J. Lumin.*, 2007, **126**, 459; (b) R. Si, Y. W. Zhang, L. P. You and C. H. Yan, *Angew. Chem., Int. Ed.*, 2005, **44**, 3256; (c) N. Zhang, R. Yi, L. B. Zhou, G. H. Gao, R. R. Shi, G. Z. Qiu and X. H. Liu, *Mater. Chem. Phys.*, 2009, **114**, 160.
- 7 (a) Y. N. Xia, Y. J. Xiong, B. K. Lim and S. E. Skrabalak, *Angew. Chem., Int. Ed.*, 2008, **47**, 2; (b) X. Y. Chen, L. Q. Liu, G. K. Liu, *J. Nanosci. Nanotechnol.*, 2008, **8**, 1126; (c) N. Niu, F. He, P. Ma, S. Gai, G. Yang, F. Qu, Y. Wang, J. Xu and P. Yang, *ACS Appl. Mater. Interfaces*, 2014, **6**, 3250.
- 8 (a) J. X. Zhu, Z. Gui and Y. Y. Ding, *Mater. Lett.*, 2008, **62**, 2373; (b) S. Y. Liu, Y. Cai, X. Y. Cai, H. Li, F. Zhang, Q. Y. Mu, Y. J. Liu and Y. D. Wang, *Appl. Catal. A: General*, 2013, **453**, 45.
- 9 (a) G. Jia, Y. J. Huang, Y. H. Song, M. Yang, L. H. Zhang and H. P. You, *Eur. J. Inorg. Chem.*, 2009, **25**, 3721; (b) L. W. Qian, Y. C. Gui, S. Guo, G. Qiang and X. F. Qian, *J. Phys. Chem. Solids*, 2009, **70**, 688; (c) J. G. Deng, L. Zhang, C. T. Au and H. X. Dai, *Mater. Lett.*, 2009, **63**, 632; (d) J. Yang, C. X. Li, Z. Y. Cheng, X. M. Zhang, Z. W. Quan, C. M. Zhang and J. Lin, *J. Phys. Chem. C*, 2007, **111**, 18148; (e) X. Wang, X. M. Sun, D. P. Yu, B. S. Zou and Y. D. Li, *Adv. Mater.*, 2003, **15**, 1442.
- 10 (a) N. Dhananjaya, H. Nagabhushana, B. M. Nagabhushana, B. Rudraswamy, C.

- Shivakumara, R. P. S. Chakradhar, *Physica B*, 2011, **406**, 1639; (b) N. Dhananjaya, H. Nagabhushana, S. C. Sharma, B. Rudraswamy, C. Shivakumara, B. M. Nagabhushana, *J. Alloys Compds.*, 2014, **587**, 755.
- 11 (a) C. K. Chang, F. Kimura, T. Kimura and H. Wada, *Mater. Lett.*, 2005, **59**, 1037; (b) N. Dhananjaya, H. Nagabhushana, B. M. Nagabhushana, B. Rudraswamy, C. Shivakumara and R. P. S. Chakradhar, *Bull. Mater. Sci.*, 2012, **35**, 519; (c) T. Thongtem, A. Phuruangrat, D. J. Ham, J. S. Lee and S. Thongtem, *CrystEngComm*, 2010, **12**, 2962; (d) L. Q. Liu, E. Ma, R. F. Li and X. Y. Chen, *Nanotechnology*, 2007, **18**, 015403; (e) S. Y. Seo, K. S. Sohn, H. D. Park, S. Lee, *J. Electrochem. Soc.*, 2002, **149**, H12; (f) L. Q. Liu, E. Ma, R. F. Li and X. Y. Chen, *J. Nanosci. Nanotechnol.*, 2008, **3**, 1398; (g) S. Y. Seo, S. Lee, H. D. Park, N. Shin, K. S. Sohn, *J. Appl. Phys.*, 2002, **92**, 5248; (h) L. Q. Liu and X. Y. Chen, *Nanotechnology*, 2007, **18**, 255704.
- 12 G. Jia, K. Liu, Y. H. Zheng, Y. H. Song, M. Yang and H. P. You, *J. Phys. Chem. C*, 2009, **113**, 6050.
- 13 (a) C. X. Li, J. Yang, Z. W. Quan, P. P. Yang, D. Y. Kong and J. Lin, *Chem. Mater.*, 2007, **19**, 4933; (b) C. X. Li, Z. W. Quan, P. P. Yang, J. Yang, H. Z. Lian and J. Lin, *J. Mater. Chem.*, 2008, **18**, 1353; (c) C. X. Li, Z. W. Quan, J. Yang, P. P. Yang and J. Lin, *Inorg. Chem.*, 2007, **46**, 6329.
- 14 G. Wang, Z. D. Wang, Y. X. Zhang, G. T. Fei and L. D. Zhang, *Nanotechnology*, 2004, **15**, 1307.
- 15 H. Cölfen and M. Antonietti, *Angew. Chem., Int. Ed.*, 2005, **44**, 5576.
- 16 (a) T. Xia, Q. Li, X. D. Liu, J. Meng and X. Q. Cao, *J. Phys. Chem. B*, 2006, **110**, 2006; (b) A. Filankembo and M. P. Pileni, *J. Phys. Chem. B*, 2000, **104**, 5865; (c) M. Wang, Q. L. Huang, J. M. Hong, X. T. Chen and Z. L. Xue, *Cryst. Growth Des.*, 2006, **6**, 1972; (d) M. Wang, Q. L. Huang, J. M. Hong, X. T. Chen and Z. L. Xue, *Cryst. Growth Des.*, 2006, **6**, 2169.
- 17 (a) Z. A. Peng and X. G. Peng, *J. Am. Chem. Soc.*, 2001, **123**, 1389; (b) Z. A. Peng and X. G. Peng, *J. Am. Chem. Soc.*, 2002, **124**, 3343.
- 18 (a) J. Yang, C. X. Li, Z. W. Quan, C. M. Zhang, P. P. Yang, Y. Y. Li, C. C. Yu

- and J. Lin, *J. Phys. Chem. C*, 2008, **112**, 12777; (b) A. W. Xu, Y. P. Fang, L. P. You and H. Q. Liu, *J. Am. Chem. Soc.*, 2003, **125**, 1494; (c) X. Bai, H. W. Song, L. X. Yu, L. M. Yang, Z. X. Liu, G. H. Pan, S. Z. Lu, X. G. Ren, Y. Q. Lei and L. B. Fan, *J. Phys. Chem. B*, 2005, **109**, 15236; (d) G. G. Li, C. Peng, C. X. Li, P. P. Yang, Z. Z. Hou, Y. Fan, Z. Y. Cheng and J. Lin, *Inorg. Chem.*, 2010, **49**, 1449; (e) X. Wang and Y. D. Li, *Chem.-Eur. J.*, 2003, **9**, 5627; (f) X. Q. Qiu, G. S. Li and L. P. Li, *J. Mater. Res.*, 2007, **22**, 908.
- 19 C. K. Chang, Q. A. Zhang and D. L. Mao, *Nanotechnology*, 2006, **17**, 1981.
- 20 (a) M. L. Pang, J. Lin, J. Fu, R. B. Xing, C. X. Luo and Y. C. Han, *Opt. Mater.*, 2003, **23**, 547; (b) G. Z. Li, M. Yu, Z. L. Wang, J. Lin, R. S. Wang and J. Fang, *J. Nanosci. Nanotechnol.*, 2006, **6**, 1416; (c) E. M. Goldys, K. Drozdowicz-Tomsia, S. Jinjun, D. Dosev, I. M. Kennedy, S. Yatsunencko, M. Godlewski, *J. Am. Chem. Soc.*, 2006, **128**, 14498.
- 21 (a) J. X. Wan, Z. H. Wang, X. Y. Chen, L. Mu and Y. T. Qian, *J. Cryst. Growth*, 2005, **284**, 538; (b) K. Y. Jung and K. H. Han, *Electrochem. Solid-State Lett.*, 2005, **8**, H17; (c) J. Yang, X. M. Liu, C. X. Li, Z. W. Quan, D. Y. Kong and J. Lin, *J. Cryst. Growth*, 2007, **303**, 480.
- 22 (a) P. Psuja, D. Hreniak and W. Strek, *J. Nanomater.*, 2007, **2007**, 81350. Z. L. Wang, H. L. W. Chan, H. L. Li and J. H. Hao, *Appl. Phys. Lett.*, 2008, **93**, 141106; (b) M. Yokoyama and S. H. Yang, *J. Vac. Sci. Technol. A*, 2000, **18**, 2472.
- 23 (a) J. H. Hao, J. Gao and M. Cocivera, *Appl. Phys. Lett.*, 2003, **82**, 2224; (b) J. H. Hao, J. Gao, and M. Cocivera, *Appl. Phys. Lett.*, 2003, **82**, 2778; (c) N. Hirosaki, R. J. Xie, K. Inoue, T. Sekiguchi, B. Dierre and K. Tamura, *Appl. Phys. Lett.*, 2007, **91**, 061101; (d) G. G. Li, Z. Y. Hou, C. Peng, W. X. Wang, Z. Y. Cheng, C. X. Li, H. Z. Lian and J. Lin, *Adv. Funct. Mater.*, 2010, **20**, 3446; (e) Q. H. Zhang, J. Wang, C. W. Yeh, W. C. Ke, R. S. Liu, J. K. Tang, M. B. Xie, H. B. Liang and Q. Su, *Acta Mater.*, 2010, **58**, 6728; (f) T. C. Liu, H. Kominami, H. F. Greer, W. Zhou, Y. Nakanishi and R. S. Liu, *Chem. Mater.*, 2012, **24**, 3486.
- 24 (a) C. Feldman, *Phys. Rev.*, 1960, **117**, 455; (b) X. M. Liu and J. Lin, *J. Mater. Chem.*, 2008, **18**, 221.

**Captions for figures and tables:**

**Figure 1.** XRD patterns of Gd(OH)<sub>3</sub>:5 mol% Eu<sup>3+</sup> products prepared at different conditions : (a) P1, pH = 9; (b) P2, pH = 11; (c) P3, pH = 9; (d) P4, pH = 11 (a,b with use of urea; c, d without use of urea). The standard data of Gd(OH)<sub>3</sub> (JCPDS No.38-1042) is shown as reference.

**Figure 2.** SEM images of Gd(OH)<sub>3</sub>:5 mol% Eu<sup>3+</sup> products prepared at the absence of urea with different pH values : (a, b) pH = 9.0 (P1); (c, d) pH = 11.0 (P2). (e-f) TEM, HRTEM and EDX images of P2 product, respectively. The inset in (f) is Fourier transform electron diffraction pattern of P2. The yellow hexagons in (b) and (f) show perfect hexagonal shape of the as-prepared Gd(OH)<sub>3</sub>:5 mol% Eu<sup>3+</sup> prisms.

**Table 1.** Parameters of the representative experiments and the morphologies and sizes of the corresponding products. All samples were treated by a homogenous precipitation process at 80°C for 2 h.

**Figure 3.** SEM images of Gd(OH)<sub>3</sub>:5 mol% Eu<sup>3+</sup> products prepared at the presence of urea with different pH values : (a, b) pH = 9.0 (P3); (c, d) pH = 11.0 (P4). (e) TEM and (f) HRTEM images of P3 product, respectively. The inset in (f) is Fourier transform electron diffraction pattern of P3.

**Scheme 1.** Illustration for the possible formation process of the hexagonal prism-like structures of Gd(OH)<sub>3</sub>.

**Figure 4.** TGA-DSC curves of Gd(OH)<sub>3</sub>:Eu<sup>3+</sup> microprisms (P2).

**Figure 5.** (a) XRD patterns of the representative  $\text{Gd}_2\text{O}_3:5 \text{ mol\% Eu}^{3+}$  product (P2□) and the standard data of  $\text{Gd}_2\text{O}_3$  (JCPDS No.12-0797). (b-e) SEM, TEM, HRTEM and SAED images of the representative P2□ product, respectively.

**Figure 6.** Photoluminescent (PL) excitation (a) and emission (c) spectra of  $\text{Gd}_2\text{O}_3:5 \text{ mol\% Eu}^{3+}$  microprisms (P2□). The inset (c) is the comparison of relative emission intensity of P1□- P4□ products ( $\lambda_{\text{ex}} = 243 \text{ nm}$ ).

**Figure 7.** BET surface area of  $\text{Gd}_2\text{O}_3:5 \text{ mol\% Eu}^{3+}$  nanoprisms (P4□) and Microprisms (P2□).

**Figure 8.** Decay curve for the  ${}^5\text{D}_0\text{-}{}^7\text{F}_2$  (613 nm) emission of  $\text{Eu}^{3+}$  in  $\text{Gd}_2\text{O}_3:\text{Eu}^{3+}$  nano-/microprisms (P1□- P4□).

**Figure 9.** (a) The cathodoluminescent (CL) emission spectra of representative prism-like  $\text{Gd}_2\text{O}_3:5 \text{ mol\% Eu}^{3+}$  phosphors (Black line, P2□; Red line, P4□) ( $V_a = 4.0 \text{ kV}$ ,  $J_a = 80 \mu\text{A}/\text{m}^2$ ). The CL intensity as a function of (b) anode current density ( $J_a$ ) and (c) anode voltage ( $V_a$ ).

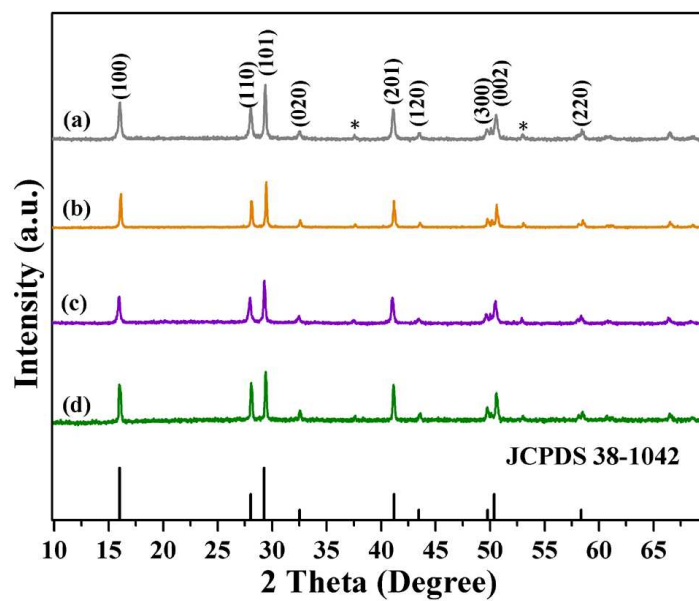


Figure 1



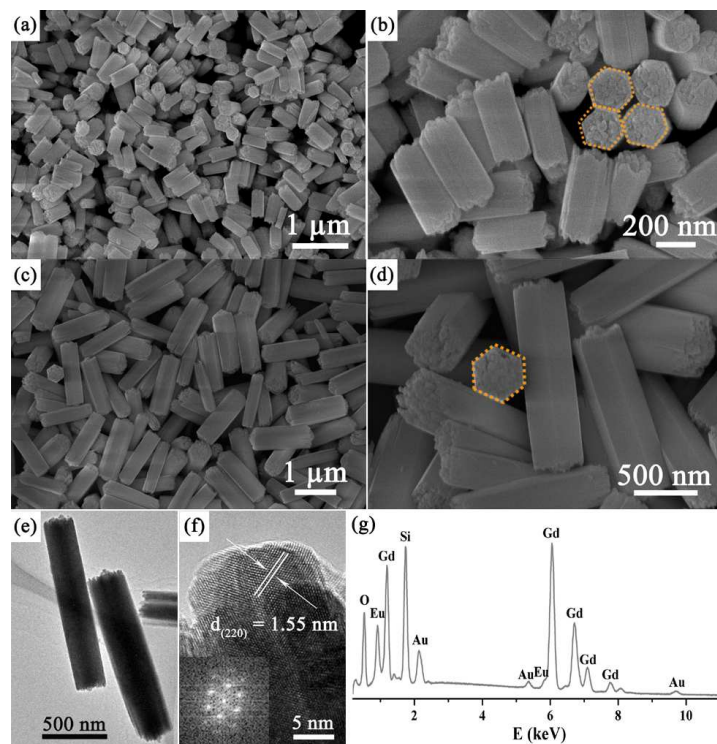
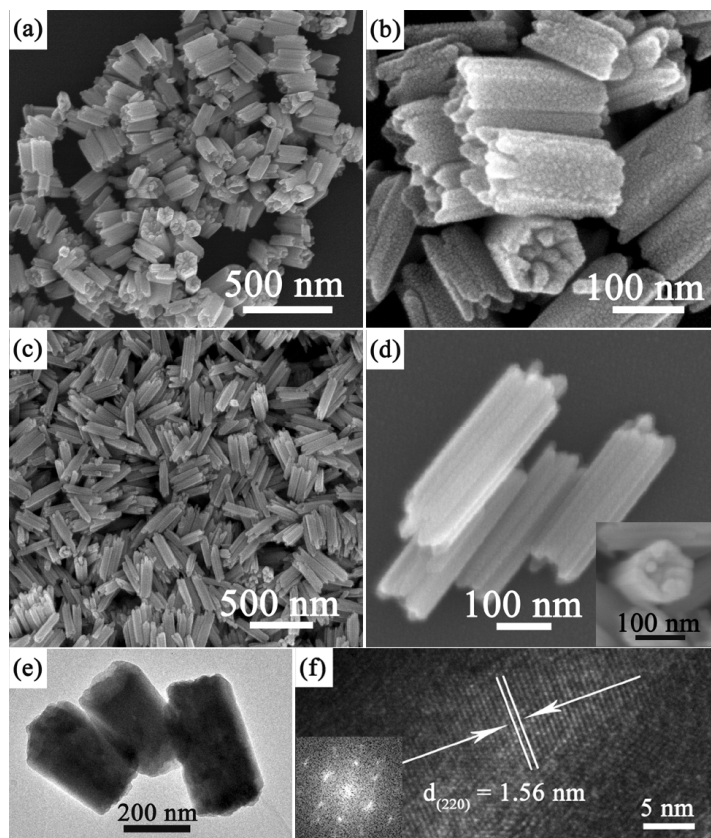


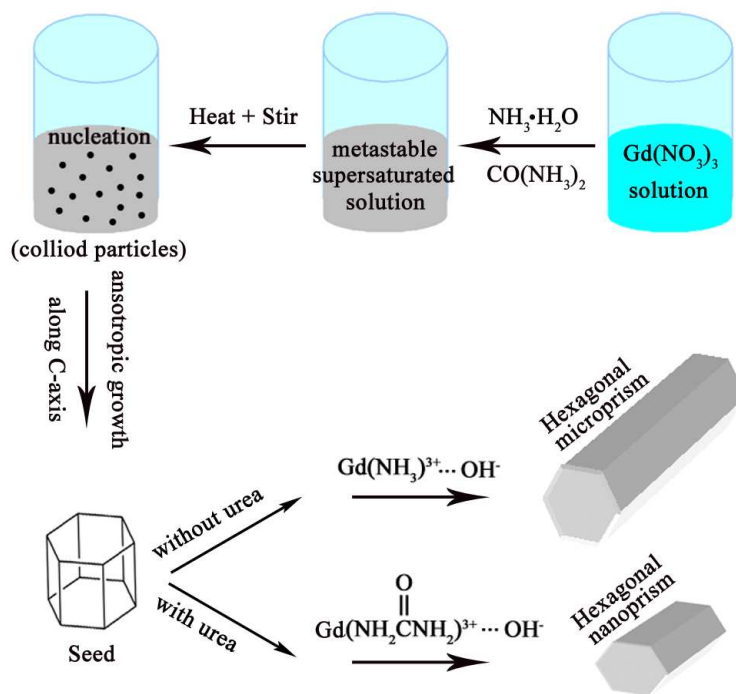
Figure 2

**Table 1**

Product	pH	$C_{\text{CO}(\text{NH}_2)_2} / \text{mol} \cdot \text{L}^{-1}$	Morphology	$L/\mu\text{m}$	$D/\mu\text{m}$	$R_{(L/D)}$
P1	9	0	hexagonal submicprisms	~0.40	0.09–0.15	2.7–4.4
P2	11		hexagonal microprisms	~1.45	0.20–0.25	5.8–7.3
P3	9	6.25	hexagonal nanoprisms	~0.20	~0.06	3.3
P4	11		hexagonal nanoprisms	~0.30	~0.065	4.6

$C_{\text{CO}(\text{NH}_2)_2}$  : The dosage of  $\text{CO}(\text{NH}_2)_2$  in the solution;  $L$ : Height of prism;  $D$ : Hexagonal side length;  $R$ : The aspect ratio equals  $L/D$ .

**Figure 3**



Scheme 1

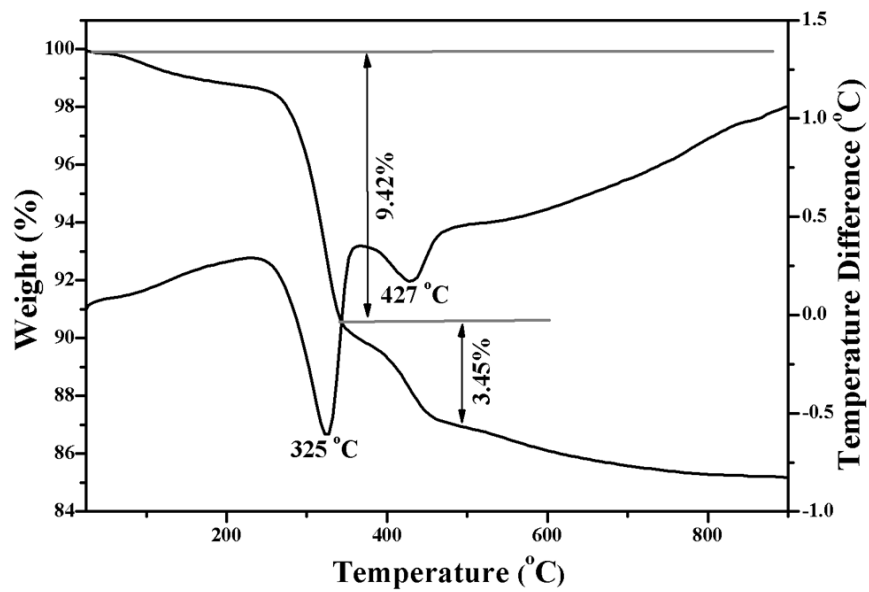


Figure 4

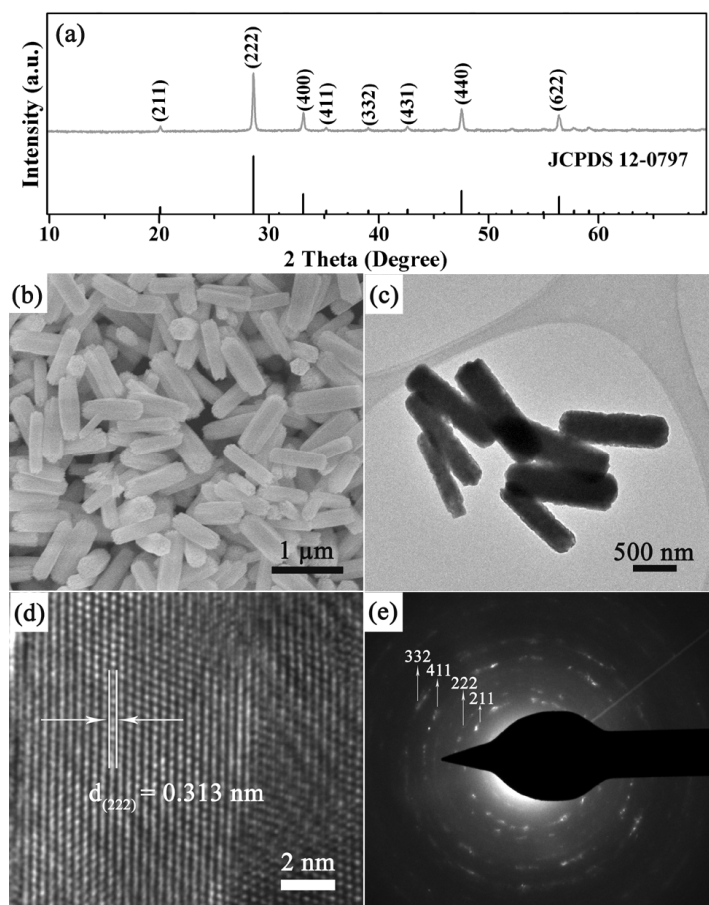
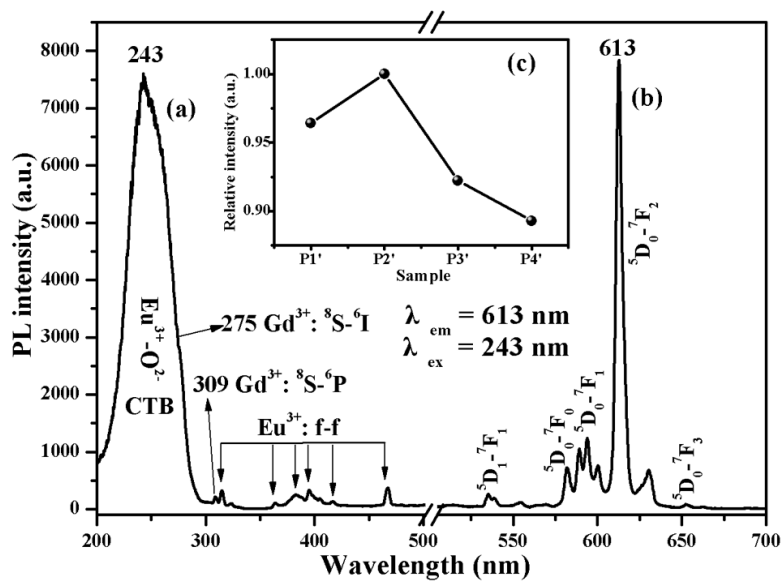


Figure 5



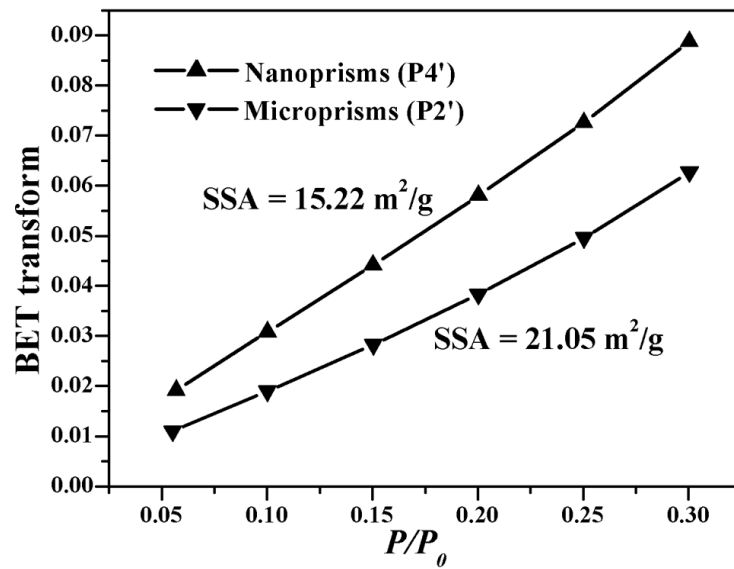


Figure 7



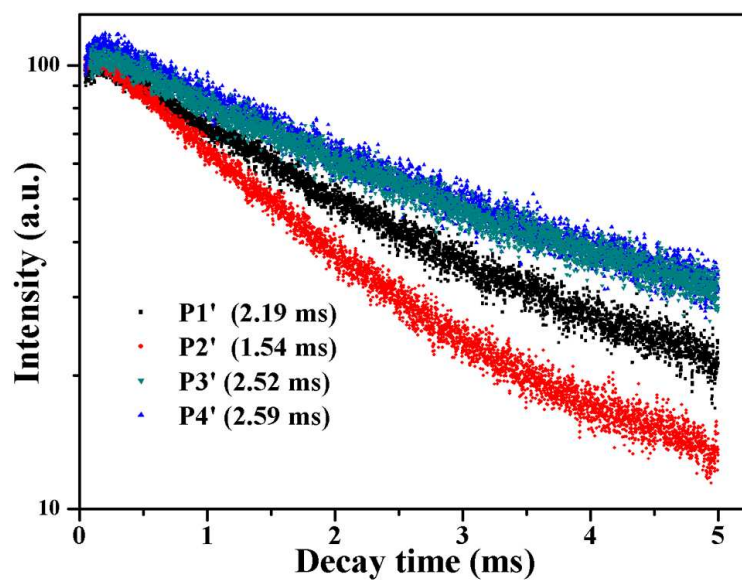


Figure 8

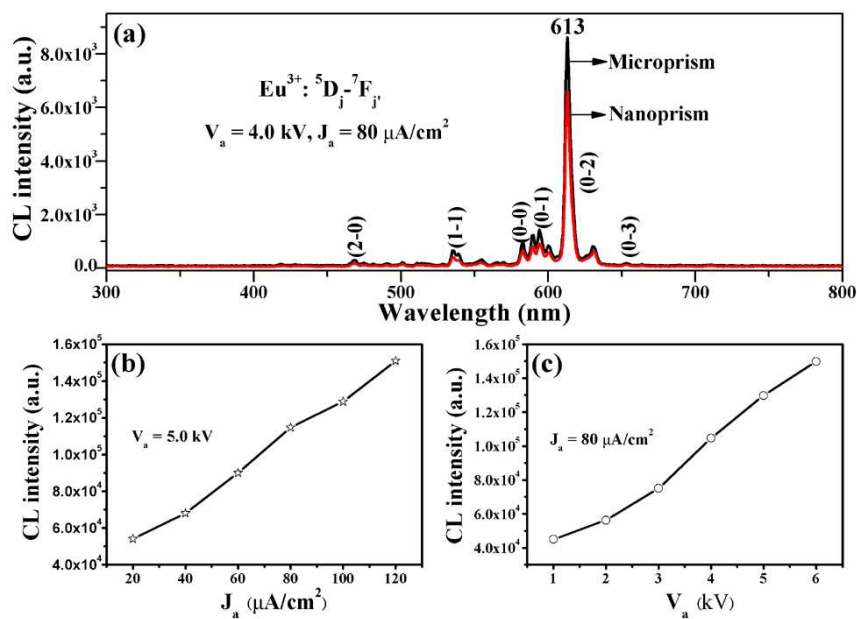
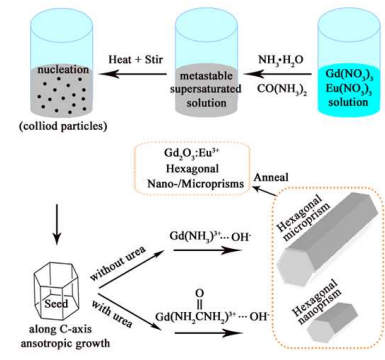


Figure 9

## A TOC Graphic &amp; Summary

<p>Guogang Li,* Yujun Liang, Mengfei Zhang and Dongyan Yu</p> <p><i>CrystEngComm</i>. xx-xxxx</p> <p><b>Size-Tunable Synthesis and Luminescent Properties of <math>Gd(OH)_3:Eu^{3+}</math> and <math>Gd_2O_3:Eu^{3+}</math> Hexagonal Nano-/Microprisms</b></p>	<p>Size-tunable <math>Gd(OH)_3:Eu^{3+}</math> and <math>Gd_2O_3:Eu^{3+}</math> hexagonal nano-/microprisms were synthesized by a facile and large scale homogenous precipitation method, and its photoluminescent and cathodoluminescent properties was investigated.</p> 
---	--